Proceedings of Montreal 2018
Global Power and Propulsion Forum
7th – 9th May, 2018
www.pps.global

GPPS-NA-2018-0109

ENGINE AIRFRAME INTEGRATION SENSITIVITIES FOR A STOL COMMERCIAL AIRCRAFT CONCEPT WITH OVER-THE-WING MOUNTED UHBR-TURBOFANS

Constance Heykena
Institute of Jet Propulsion and Turbomachinery, Technische Universität Braunschweig
c.heykena@ifas.tu-braunschweig.de
Braunschweig, Germany

Luciana Savoni
Institute of Aerodynamics and Flow Technology, Deutsches Zentrum für Luft- und Raumfahrt e.V
luciana.savoni@dlr.de
Braunschweig, Germany

Jens Friedrichs
Institute of Jet Propulsion and Turbomachinery, Technische Universität Braunschweig
j.friedrichs@ifas.tu-braunschweig.de
Braunschweig, Germany

Ralf Rudnik
Institute of Aerodynamics and Flow Technology, Deutsches Zentrum für Luft- und Raumfahrt e.V
ralf.rudnik@dlr.de
Braunschweig, Germany

ABSTRACT

A transport aircraft concept featuring over-the-wing-mounted nacelles (OWN) positioned aft of the wing's trailing edge is investigated with numerical methods. The objective of the study is to compare two different approaches for integrating the nacelle to the airframe from an aerodynamic point of view. On one hand, a pylon mounted OWN configuration is chosen for installing the propulsion system. On the other hand, a closer coupling between wing and nacelle by embedding the OWN into the wing is examined. Both configurations will be analysed at a representative reference position and discussed in terms of similarities and differences. Afterwards, a positioning study with a free flying nacelle is conducted to explore the aerodynamic sensitivities of wing and nacelle for this engine airframe integration position. The results show that a favourable position with the potential for drag reduction can be found.

INTRODUCTION

The study lies within the framework of the Collaborative Research Centre (CRC) SFB 880 which focuses on fundamental and applied research on technologies for future high lift aircrafts (Delfs et al., 2017), (Radespiel et al., 2017). Driven by the demand for a drastic reduction in noise emission and fuel consumption, which was claimed by the ACARE goals (European Commission, 2011), the investigated transport aircraft concept aims to provide technologies for a cruise efficient aircraft with short take-off and landing capabilities enabled by an active high lift system. The configuration design itself is one of the most interesting features of this concept. Nacelles installed on the wing offer enough space for growing engine sizes when increasing the bypass ratio (BPR) of turbofan engines while having simultaneously a positive effect on the aircraft noise due to e.g. shieling effects. A major drawback of OWN arrangements is the aerodynamic behaviour which is known to lead to a higher overall airframe drag with respect to common under-the-wing turbofan installations. However, recent studies have shown, that OWN can offer the potential to improve aerodynamic performance especially for rising BPR and corresponding increasing engine dimensions (Hooker et al., 2013). When the nacelle is placed at the wing's trailing edge at high cruise velocities the engine inlet stream tube strongly influences the flow field of the wing by slowing down the approaching flow. As a result, the strength of the shock that is observed on the suction side of the wing for the clean wing configuration at the cruise Mach number will be reduced. Here lies a potential benefit for a better overall aircraft performance at high speed conditions.

Transport Aircraft concept

The transport aircraft concept investigated in this study is sized for 100PAX with a maximum payload of 12t. It is a short to mid-range aircraft with a design mission range of 2,000 km. The active high-lift system enables the aircraft to take-off and land within 900m runway length. It is a low wing configuration with a length of 30.9m and 28.745m span width. The wing has a reference area of 99m^2 and since the

design cruise speed lies at Ma = 0.78 a sweep angle of 26 deg. The aircraft is powered by two geared ultra-high bypass ratio (UHBR) turbofan engines, which will be installed over-the-wing aft of the wing's trailing edge. The position of the engine is at 31% of the span on each wing. This position also hosts the main landing gears. Further details on the transport aircraft can also be found in Heinze and Weiss, 2015. Figure 1 shows an overview of the aircraft concept.

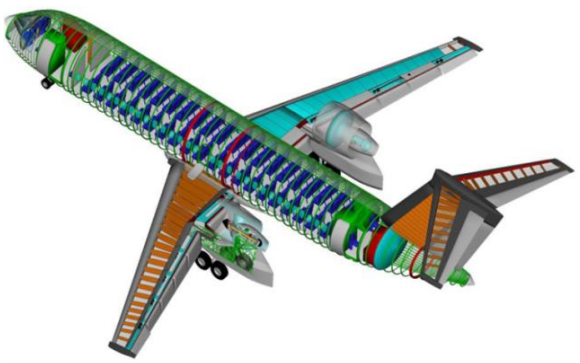

Figure 1 Overview of STOL A/C concept

UHBR-engine

The BPR and fan diameter of turbofan engines are continuously increasing to improve propulsion efficiency and hence reduce fuel consumption. This is why for the presented A/C concept an UHBR engine was chosen. By increasing the fan the dimensions of the nacelle will rise as well. This will lead to more weight and wetted area, which is directly coupled with drag generation. To benefit from the gain in engine efficiency, a sophisticated engine airframe installation becomes crucial. Otherwise the benefit coming from the engine will be eliminated due to the nacelle size in the overall balance of the configuration.

For the design of the engine, the thrust requirements were derived from the aircraft's mission profile since this force needs to be supplied by the propulsion system. The engine design point was at top of climb. The thermodynamic design of the jet engine was done with the commercial performance tool GasTurb (Kurzke, 2012). Driven by reducing SFC, the BPR was set to 17 at the design point. Moreover, it is a geared turbofan with separated nozzle as can be seen in Figure 5. The engine cycle design also determines relevant dimensions like the fan inlet and nozzle outlet areas for instance, which serve as an input for the CFD surface model design. Additionally, the engine cycle also delivers thermodynamic parameters like mass flow rate, pressure and temperature for each operating point, which are required as an input for the engine boundary conditions during the numerical study.

Engine Airframe Integration

For the integration of the aircraft engine to the airframe, two approaches are investigated, which are illustrated in Figure 2. On the left hand side, a pylon mounted configuration is shown, which will be declared as Wing-Body-Engine-Pylon (WBEP) configuration in the following. The other side of the A/C in Figure 2 shows the configuration which aims for embedding the propulsion system into the wing. This configuration is called Wing-Body-Embedded-Engine (WBEE). For both concepts, a relevant starting position was chosen and their high speed behaviour analysed.

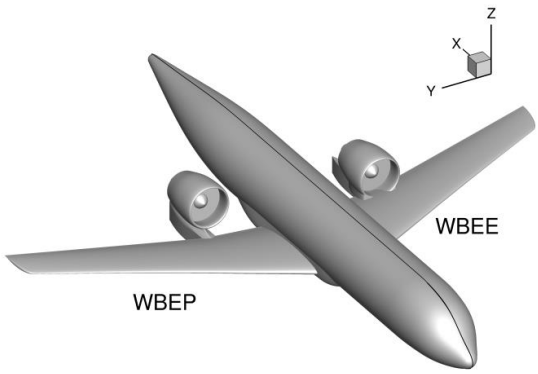

Figure 2 A/C model with different nacelle integration concepts on each wing

METHODOLOGY

Two different approaches for the integration of the UHBR nacelle are to be compared in terms of high speed performance. Both configurations have a different reference position. For the WBEP, the nacelle is placed with the highlight area, at which the flow enters the nacelle, at the trailing edge. Hooker et al., 2013 found this position to be a favourable OWN position. It has been confirmed in Savoni and Rudnik, 2106 for the CRC WBEP concept. Figure 3 shows the cross section of the WBEP through the engine axis at the relative spanwise position η = 0.31. The nacelle is mounted with a pylon to the wing having an installation angle of 3 deg. This position also accommodates an under the wing fairing for the landing gear. A detailed discussion on the design of the WBEP can also be found in Savoni and Rudnik, 2018.

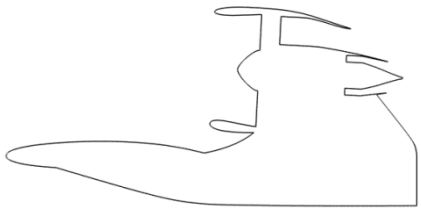

Figure 3 Section at η = 0.31 for WBEP

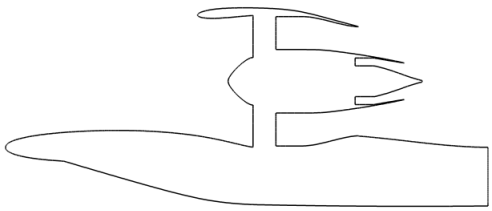

Figure 4 Section at η = 0.31 for WBEE

For the WBEE, the nacelle is placed with the fan face being at the trailing edge of the wing. The minimum in vertical direction of the fan diameter is located right above the wing surface. In a first approach, no installation angles are implemented. One assumption which led to the design shown in Figure 4 is that the minimal impact of the nacelle on the wing is to be analysed. This means that the wing shape is kept constant while the isolated nacelle model is trimmed and a junction between wing, nacelle and landing gear is designed In addition, previous studies have shown, that the further down the embedded nacelle is placed the better the high speed performance becomes in terms of AoA and drag. A detailed discussion on the WBEE can also be found in Heykena and Friedrichs, 2018.

Figure 2 shows the final surfaces model geometry for both configurations, which were analysed with numerical methods. Since the focus lies on the aerodynamic interaction of nacelle and Wing-Body (WB), the tailplanes were omitted at this stage of the project as can be seen in Figure 2. Aircraft stability and control analysis of the A/C concept are subject to future investigations.

Positions of free flying engine study

To explore the effect of the over-the-wing nacelle on the CRC 880 A/C concept with respect to the aerodynamic behaviour of wing and nacelle a parameter study with varying engine positions is conducted. In Savoni and Rudnik, 2016, the differences between the WBEP and free flying engine results have been discussed for one position leading to the results that the model of the free flying engine is sufficient to gather a basic understand in the aerodynamic behaviour of this configuration. In correspondence with the nomenclature, the free flying engine simulation will be referred to as WBE.

The considered parameter space is aft of the wing's trailing edge. The green dots in Figure 5 illustrate the position of the nacelle, which were examined. The upper trailing edge point was chosen as a reference point for the wing. The reference point of the engine lies on the fan face. Instead of the engine axis, the minimum in vertical direction of the outer fan diameter was chosen, also indicated by the green point in Figure 5.

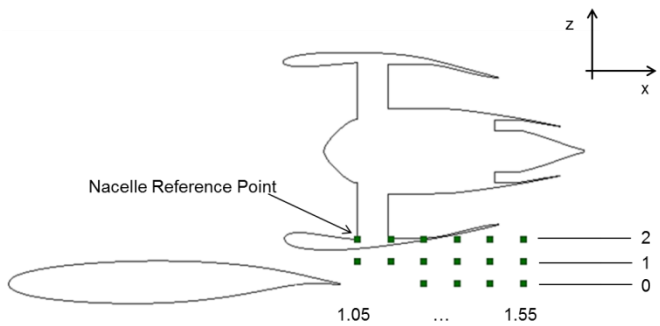

Figure 5 Free flying engine positions

Three heights were considered. The first is with the engine reference point on the same level as the trailing edge. For the second and third height, the nacelle was shifted up by 12.5% and 25% of the fan diameter, resp. The vertical positions are declares as z = 0, 1 and 2 in the following. The axial positions of the nacelle are equally distributed and last from x = 1.05 to 1.55 with respect to the local wing chord. The spanwise position remains constant at $\eta = 0.31$ within this study.

To evaluate the results of the OWN integration, simulations of the clean WB and isolated engine will be conducted as well.

Numerical Approach

The surfaces models required for the numerical study were created with the commercial CAD software CATIA V5R21. To safe computational resources all simulations on the A/C model were carried out on a half model applying a symmetry boundary condition. For the free flying engine studies, the landing gear box was also not implemented in the surface model due to its close coupling with the nacelle for both configurations.

Grid Generation

Computational grids were generated with the commercial grid generator centaur (CentaurSoft, 2017). All computational grids were hybrid using triangles to discretize most of the surfaces while structured elements were used for blunt trailing edges of wing and nacelle. A prism layer of 37 was built upon the surfaces choosing the first cell thickness to match a dimensionless wall distance $y^+ \approx 1$. The growing rate of the prism layers was set to 1.23. Afterwards, the farfield was filled with tetrahedron and pyramids. Local refinements and cell clustering was applied in crucial areas like leading and trailing edges. Special focus has be set to the mesh uniformity and resolution at the engine inlet and outlet planes, which is necessary for the solver to resolve the engine flow at these parts of the grid correctly.

Since the setup can be easily adapted for different engine positions every case investigated in the WBE study was meshed and no mesh deformation was deployed. This feature of the software ensures the mesh comparability for different engine positions. Final mesh sizes were around 9 million nodes for the WB, 5 million for the isolated engine and about 21 million for the aircraft configurations including the engine.

CFD solver

The flow simulations were carried out using the DLR TAU code. It is based on a finite-volume approach for solving the Reynolds-averaged Navier-Stokes (RANS) equations for unstructured grids. (DLR, 2014) For the time integration, the implicit lower-upper symmetric Gauss Seidel (LU-SGS) scheme was used for all considered cases. For the podded configuration, a central scheme was applied. Turbulence was modelled with the one equation model proposed by Spalart and Allmaras in its negative formulation (SA-neg). (Allmaras et al., 2012) An upwind schema was used for the embedded nacelle case and Menter's two equation shear stress transportation (SST) model was deployed for turbulence modelling. (Menter, 1994)

Separations occurred for the WBEE on both sides of the nacelle. Due to stability reasons the setup was changed. The latter setup is also applied for the WBE study.

Boundary conditions

Within this investigation the high speed behaviour is evaluated. This is the reason why, the considered flight condition for all simulations is the steady cruise condition. The speed of flight is Mach 0.78 at an altitude of 11,277m and the free stream conditions were set accordingly. All aircraft simulations were run with a target lift constraint of 0.46 and the corresponding angle of attack α needed to reach this lift was determined iteratively. At this state of flight, the overall aircraft design predicts a thrust requirement of 16 kN. The propulsion system is to provide this thrust, which determines the mass flow rates, total pressure and total temperature for the engine boundaries treatment.

Viscous walls were considered to be fully turbulent without transition since the Reynolds number for the tested case is about 21×10^6. The engine fan face is treated as an outlet boundary condition. The mass flow rate entering the engine was applied on this plane. This boundary condition benefits by contrast of a static pressure boundary condition if inlet distortions are present and should be captured as well. Since the aircraft engine model features a separated nozzle, the hot core and cold bypass exhaust planes were treated as subsonic inlet boundary conditions. Both, a total pressure and total temperature ratio were applied on both nozzle exit planes. The parameters for the engine inlet and outlet were kept constant for all simulations meaning that there was no adaption of the thrust setting for the integrated nacelle.

RESULTS AND DISCUSSION

In the following section, the results of the reference WB and isolated engine are shown, followed by the discussion of the WBEP and WBEE results. Afterwards, the placement study results for the WBE study are discussed.

Baseline Results

For the integration studies, the clean WB and isolated engine are taken as a reference for the evaluation of the integrated nacelle and WBE simulation results. In Figure 6 the pressure distribution and skin friction lines on the upper wing is shown. The clean wing has a shock at about 75 % of the wing chord which extends from the wing root to tip. Further, the skin friction lines reveal a trailing edge flow separation in the area of the kink of the wing, where the nacelle will be placed.

The resulting angle of attack equals 2.04 deg for target C_L. With respect to drag, the internal drag estimation of the solver predicts 252 drag counts for the WB. The isolated engine was simulated without an angle of attack. The lift generated by the nacelle during this operation point is negligible. The total drag, including also the inner surfaces like nozzle ducts of the nacelle, results in 225 drag counts. For the analysis of the engine airframe integration, the isolated engine will also be simulated for different flow angles.

WBEP vs. WBEE

Installing the engine in an over-the-wing position strongly influence the pressure distribution on the suction side of the wing and on the nacelle for both configurations, as can be found in Figure 6. The clean WB is compared to the WBEP (left) and WBEE (right). The resulting AoA for the WBEP to reach target C_L rises to 3.7 deg and 3.9 deg for the WBEE. The results of WBEP and WBEE in Figure 6 show that there are differences of the engine installation effect between both configurations. One reason is for sure that the engine position is not exactly the same. As described in the methodology chapter, the axial and vertical reference positions of the nacelle were chosen to be different. For the WBEP, the nacelle is placed with the highlight area at the trailing edge of the wing, while for the WBEE configuration the nacelle is partly located on the wing.

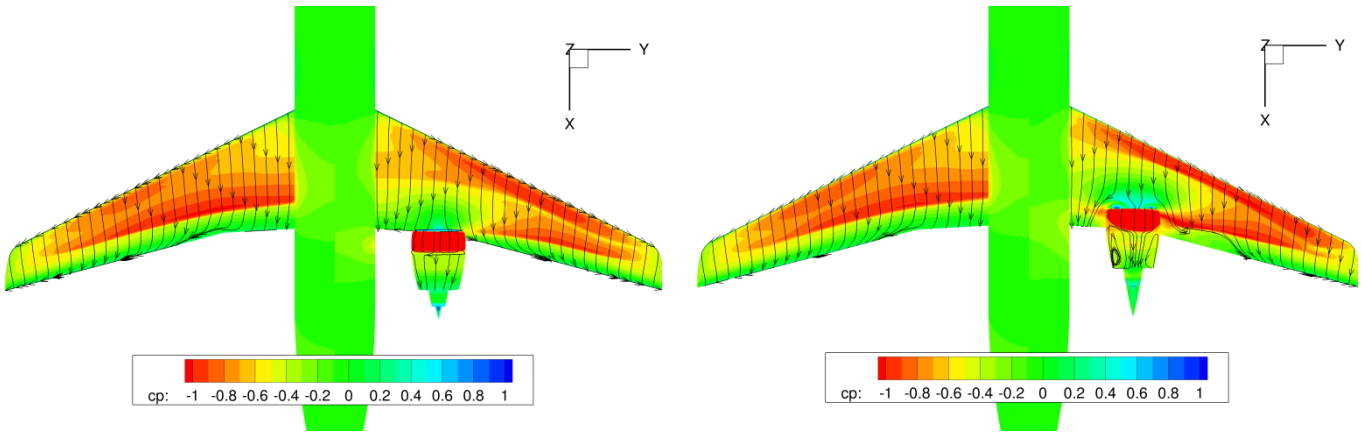

WBEP **WBEE**

Figure 6 Pressure distribution and skin friction lines for WB and integrated nacelle

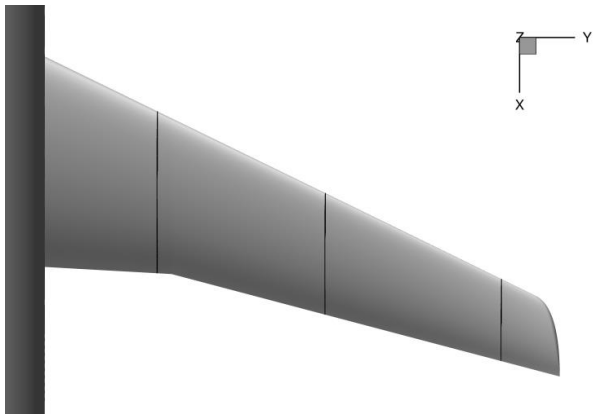

Positions of cuts

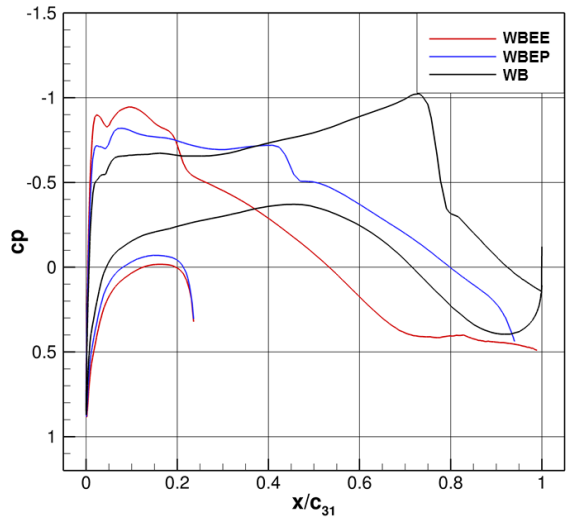

η = 0.31 (engine axis)

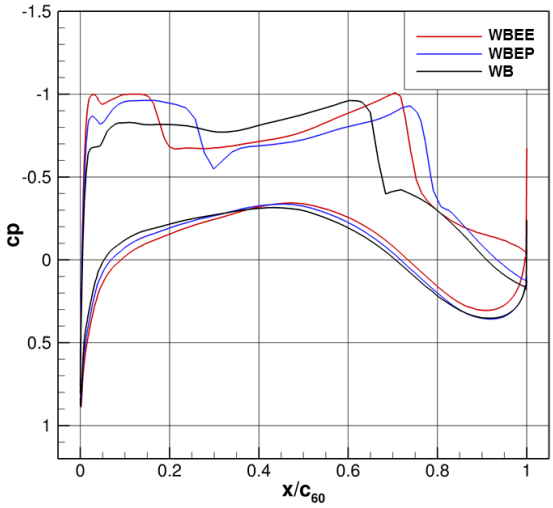

η = 0.6

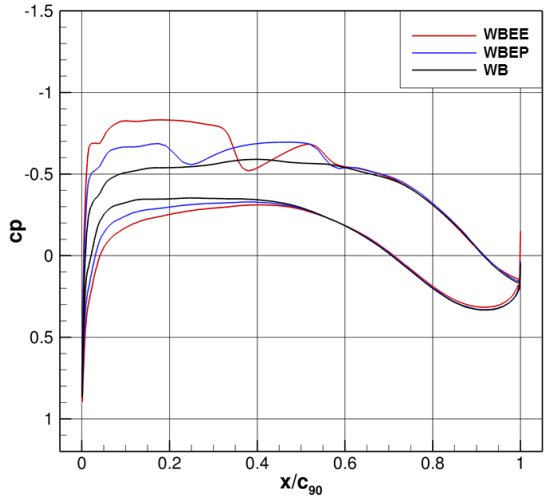

η = 0.9

Figure 7 Sectional c_p distribution of wing at target C_L (WB; WBEP; WBEE)

Impact on Wing

In general, the approaching flow will be decelerated on the inner part of the wing due to the presence of the nacelle. The shock, which can be found on the clean wing, becomes mitigated and shifted upstream. Instead of one shock, a double shock can be found on the outer part of the wing.

As soon as the flow passes the highlight area of the nacelle, it becomes accelerated again leading to a shock close to the nacelle on both sides. Further, the decelerating effect of the embedded nacelle appears to be stronger than for the WBEP. A possible reason for this lies in the nature of an embedded nacelle. For the podded configuration the flow can pass the nacelle on 360 degrees (despite from the blocking of the pylon). If the nacelle will be connected to the wing directly, there will be no gap between wing a lower nacelle anymore leading to a stronger ram air effect of the approaching flow.

The differences become also obvious, when looking at the sectional pressure distribution in Figure 7. At the section through the engine axis at η = 0.31 the c_p plot indicates, that the WBEE has a shock at 20% of the wing chord. The WBEP's shock position is located at 45% chord length, also being not as intense as for the WBEE. In addition, the loss in lift generation at this section is less for the WBEP when comparing the results with the WBEE. In addition, the flow separation being present for the clean wing will be suppressed by the presence of the nacelle due the acceleration of the flow between lower nacelle lip and wing trailing edge. At the η = 0.6 section the double shock due to the engine installation becomes evident for both configurations. For the WBEE, the second shock even results in a shock induced separation, which is also indicated by the skin friction lines in Figure 6 (right). An outboard section at η = 0.9 reveals that the outer part is aerodynamically higher loaded with respect to the clean wing to compensate for the lack of lift generation on the inner part of the wing.

Impact on Nacelle

Installing the nacelle at this position has also a strong impact on the flow around the nacelle and its corresponding pressure distribution. For an OWN, the surrounding flow field will be influence by the presence of the wing leading to a different flow situation with reference to the isolated nacelle. The skin friction lines on the nacelle of the WBEP in Figure 6 indicate the beginning of a shock induced flow separation on the upper part of the nacelle for this operating point. Looking at the skin friction lines for the WBEE on the other side, large areas with detached flow on both sides of the nacelle can be observed. These separations are caused by the design of the intersection between wing and nacelle. Eliminating the root cause for these separations will be a major challenge in the design of embedded propulsion systems and subject to a future investigation on the nacelle design.

Due to the occurring flow separation on the nacelle of the WBEE, only the sectional c_p distribution of the 12 o'clock position of the nacelle will be examined. In Figure 8, the integrated nacelles of WBEE and WBEP (solid lines) are compared to isolated nacelle solutions (dashed lines). Following the methodology described in Hooker et al., 2013, the isolated nacelle simulations were run for the same angle of attack as each full configuration's resulting AoA at target C_L. For the WBEP, the installation angle of 3 deg. was added to the aerodynamic angle of 3.7 deg.

The pressure contours for both cases reveal a change in local incidence angle of the nacelle profile at this section. The clean nacelle operating under an AoA has in both cases a stronger suction peak leading to an acceleration which results in a shock at 20% of the nacelle chord for 3.9deg and 15% for 6.7deg. By installing the engine, the suction peak becomes lower and the position of the shock is shifted downstream. This means from the engine's point of view, the installation to the airframe has a positive effect on the nacelle flow at this section of the nacelle.

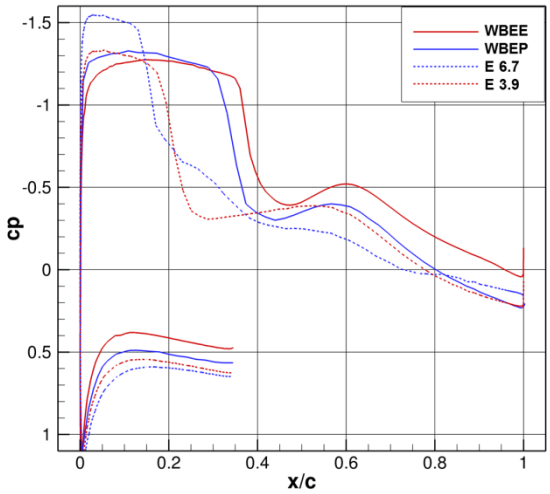

Figure 8 Sectional c_p distribution of nacelle for WBEE, WBEP and engine (E) under AoA

Impact on Engine Inflow

A distinct difference between the engine airframe integration approaches is the boundary layer ingestion (BLI) of the WBEE. In Figure 9, the normalized total pressure shows the thickness of the boundary layer at the section through the engine axis. It becomes evident, that for this integration method not just the flow on the cowling of the nacelle will be influenced. There will also be a severe impact on the fan flow. The boundary layer ingested by the engine spreads almost over half of the span the lower fan face part in the depicted section.

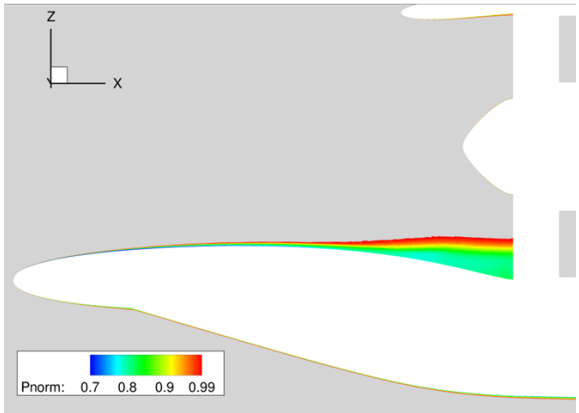

Figure 9 Boundary layer for WBEE at η = 0.31

The comparison between both configurations shows, that the flow phenomena taking place on the upper wing's surface resemble one another with respect to the mitigation of the shock on the inner wing. This phenomenon holds the potential for wave drag reduction for OWN. Further, both designs have the double shock on the outboard part of the wing, which is to be further investigated by a shape design optimisation of the wing. In addition, WBEP and WBEE show the change in local incidence of the flow approaching the nacelle, which is one potential benefit of the OWN configuration with respect to the nacelle design compared to conventional configurations.

Apart from the parallels, each configuration aims for different ways in reducing drag. While the podded WBEP configuration will benefit from positive installation effects on the lower nacelle lip, which have been showed in Savoni and Rudnik, 2016 and will shortly be discussed in the next section, the second configuration aims for decreasing the wetted area of the UHBR nacelle by embedding it into the wing. Besides, a closer coupling with the wing could possibly reduce the intake length which would counterbalance the weight penalty due to the increasing dimensions of the UHBR nacelle. The inevitable BLI of this concept is another challenge, not only in terms of design and distortion at the fan face, but also for the evaluation of overall performance for this configuration. Due to the BLI of the WBEE, the distinction between thrust and drag is not as explicit as for the WBEP. For future performance assessment and comparison of both concepts, for instance a mechanical energy based analysis as proposed by Drela, 2009 or exergy-based assessment as shown in Arntz et al., 2015 becomes necessary.

Free flying engine sensitivities

To gather a deeper understanding in the fundamental aerodynamic behaviour of the over-the-wing nacelle position for the CRC880 A/C concept is the objective of the free flying engine simulations. The simulation results for the conducted parameter variation in terms of AoA are summarized in Figure 10. It can be observed that with increasing axial position of the nacelle, the AoA to reach target C_L decreases. Further, the differences between the investigated heights of the nacelle diminish with increasing x-position.

In accordance with the AoA, Figure 11 outlines the resulting overall drag values for each nacelle position. When the inlet of the nacelle is still above the wing as illustrated in Figure 5, separations occur on wing and nacelle due to the acceleration of the flow within the gap between both components. Especially for the installation position x =1.05, the areas with detached flow on the nacelle are the key drivers for the high drag of these configurations. Because of this flow phenomenon, a position further downstream becomes more favourable. For all three heights being tested a minimum can be found at an axial position of 1.35 of the local wing chord. For the rearmost position, the results for C_D and AoA hardly differ anymore.

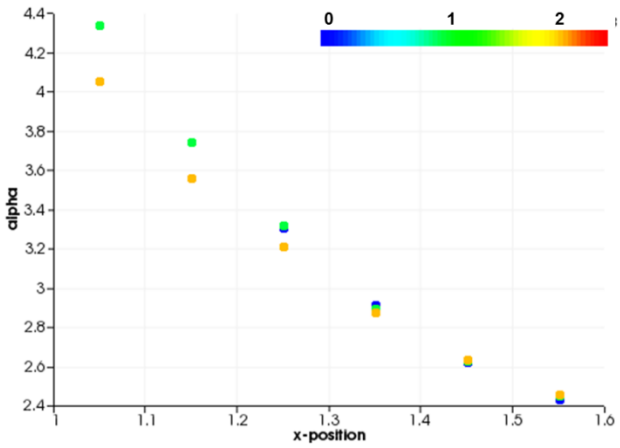

Figure 10 AoA for nacelle placement study

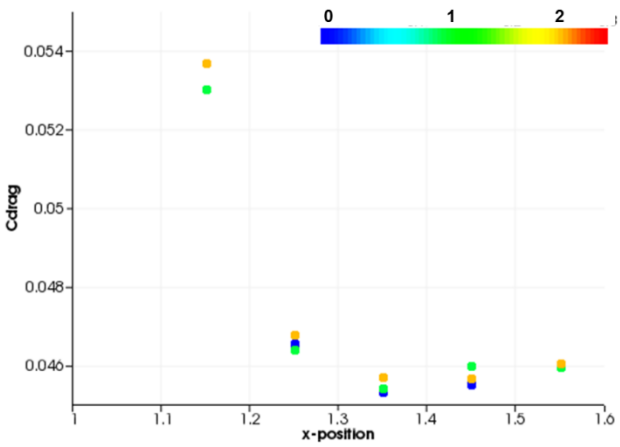

Figure 11 C_D for nacelle placement study

A thrust/drag analysis has also been performed for each nacelle position with the DLR in-house tool AeroForce (Wild, 1999). This tool offers the possibility to break the forces acting on aircraft configurations down into several A/C components and distinguish between aerodynamic and propulsive surfaces. According to Hooker et al., 2013 for instance, surfaces inside the engine inlet stream tube and exhaust duct belong to the propulsion thrust. Surfaces outside of the engine inlet stream tube contribute to the aerodynamic surfaces and will be considered for the drag bookkeeping.

Figure 12 shows the amount of drag which is generated for all surfaces being part of wing (W), body (B) and the cowling of the engine (E) aft of the nacelle stagnation line. The three heights which are investigated are indicated as shown in Figure 5.

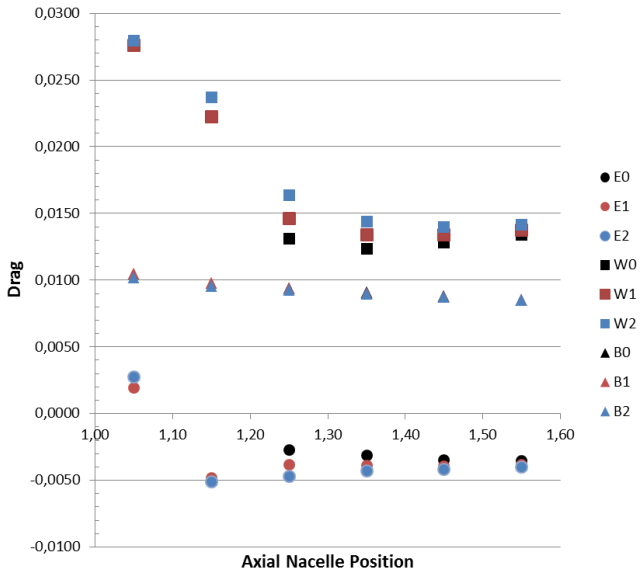

Figure 12 Results of thrust/drag bookkeeping for WBE

While the drag of the wing is relatively high for a position with the nacelle above the wing due to the already mentioned separations, the drag decreases when shifting the nacelle downstream. Especially for position with the lower lip of the nacelle close to the trailing edge of the wing (x = 1.25) a positive interaction of wing and nacelle can be observed. The vertical nacelle position influences the amount of drag caused by wing and nacelle. The lower the engine is placed the lower the amount of drag generated by the wing while the amount driven by the nacelle increases and vice versa.

The drag considerations for the free flying engine show the benefit of OWN. A negative value for the nacelle indicates, that the nacelle cowling does not generate drag, but thrust. The x = 1.25 position shows, that by changing the gap size between wing trailing edge and lower nacelle lip for the different z-positions, the positive installation effect on the engine can be increased. However, at the same time the drag of the wing rises as well. Another finding of the study is, that when the lower lip is placed in the wake of the wing (z = 0), the thrust generating installation effect of the nacelle

vanishes. This means the acceleration of the lower lip is necessary to benefit from the OWN.

CONCLUSIONS

For two different engine airframe integration approaches a chosen reference position has been investigated with CFD methods. The results show, that both configurations show a strong interaction between the upper wing and nacelle. In addition, a positive effect on the upper lip of the nacelle local flow incidence can be observed. This influence of the wing flow field on the nacelle intake might also be favourable for the low speed operation and might also hold the potential for a short nacelle intake design for UHBR engines to deal with increasing weight and wetted area issues connected to this engine type.

A free flying OWN placement study showed that there is a parameter space for the nacelle position, which has the potential for minimizing the overall drag due to a positive installation effect of the nacelle. However, this benefit might only be applicable for a podded nacelle configuration since it is mainly driven by accelerating the flow on the lower lip of the nacelle. For the embedded nacelle, the outcome of the placement study is necessary for deriving findings on the nacelle flow in the flow regime of the wing. This knowledge will lead to a future design update for embedded configuration to eliminate the flow separation on the nacelle.

In addition, the outcome of the study outlines that especially for the design of OWN configurations it will be crucial not to design wing and nacelle shape separately as it was done during this study. Instead, for a proper configuration design and in particular for the embedded nacelle, the interaction of nacelle and wing needs to be taken into account during a shape optimisation to solve e.g. the double shock on the outer part of the wing, which was present for all considered test cases.

NOMENCLATURE

Abbreviations

A/C	Aircraft
ACARE	Advisory Council for Aeronautics Research in Europe
AoA	Angle of Attack
B	Body
BPR	Bypass Ratio
BLI	Boundary Layer Ingestion
CFD	Computational Fluid Dynamics
CRC	Collaborative Research Centre
Deg	degree
E	E
OWN	On-Wing-Nacelle
PAX	Passengers
RANS	Reynolds Averaged Navier Stokes
SFC	Specific Fuel Consumption
STOL	Short Take-off And Landing
UHBR	Ultra-High-Bypass Ratio
W	Wing
WB	Wing-Body
WBE	Wing-Body-Engine
WBEE	Wing-Body-Embedded-Engine
WBEP	Wing-Body-Engine-Pylon

Symbols

α	Angle of Attack
η	Non-dimensional longitudinal dimension
c	Chord length
C_D	Drag coefficient
C_L	Lift coefficient
c_p	Pressure coefficient
Ma	Mach number
x	axial position
z	vertical position

ACKNOWLEDGMENTS

Financial support has been provided by the German Research Foundation (Deutsche Forschungsgemeinschaft – DFG) in the framework of the Collaborative Research Center SFB 880. Computational Resources have been provided by the North-German Supercomputing Alliance (HLRN). The authors would like to thank Arno Ronzheimer for his valuable support on the CAD aircraft design.

REFERENCES

[1] Arntz, A., Atinault, O., Merlen, A., "Exergy-Based Formulation for Aircraft Aeropropulsive Performance Assessment: Theoretical Development", AIAA Journal, Vol. 53, No. 6, pp. 1627-1639, 2015

[2] Allmaras, S. R., Johnson, F. T., and Spalart, P. R., "Modifications and Clarifications for the Implementation of the Spalart-Allmaras Turbulence Model," ICCFD7-1902, 7th International Conference on Computational Fluid Dynamics, Big Island, Hawaii, 9-13 July 2012

[3] CentaurSoft, 2017, www.centaursoft.com

[4] Delfs, J, Appel, C, Bernicke, P, Blech, C, Blinstrub, J, Heykena, C, Kumar, P, Kutscher, K, Lippitz, N, Rossian, L, Savoni, L, Lummer, M "Aircraft and technology for low noise short take-off and landing", 2017, 35th AIAA Applied Aerodynamics Conference Denver, Colorado

[5] DLR "TAU-Code User Guide", Release 2014.1.0, 2014, DLR

[6] Drela.M. "Power Balance in Aerodynamic Flows", AIAA Journal, Vol. 47, No. 7, pp. 1761-1771, 2009

[7] European Commission "Flightpath2050 – Europe's Vision for Aviation, Report on the High Level Group on Aviation Research", ISBN 978-92-79-19724-6, 2011, www.acare4europe.org

[8] Heinze, W and Weiss, T, "Main Data Sheet. A/C Type: SFB 880 Reference Aircraft REF3", 2015, Project Data Sheet

[9] Heykena, C and Friedrichs, J., "Aerodynamic Investigation of an embedded UHBR-Engine Concept" Proceedings of GPPS Forum 18, Global Power and Propulsion Society, Zurich, 10th-12th January 2018

[10] Hooker, JW, Wick, A., Zeune, C, and Agelastos, A, "Over Wing Nacelle Installations for Improved Energy Efficiency" 31st AIAA Applied Aerodynamics Conference, San Diego, CA, 2013

[11] Kurzke, J., GasTurb 12 - Design and Off-Design Performance of Gas Turbines, 2012
[12] Menter, FR, “Two-equation eddy-viscosity turbulence models for engineering applications”, AIAA Journal, 1994, Vol. 32, No. 8
[13] Radespiel, R, Bertsch, L, Heinze, W, “High-Lift Research for Future Transport Aircraft”, 2017 DLRK Munich
[14] Savoni, L. and Rudnik, R., “Aerodynamic Assessment of Pylon-Mounted Over-the-Wing Engine Installations on a STOL Commercial Aircraft Concept”, In book: New Results in Numerical and Experimental Fluid Mechanics XI, Contributions to the 20th STAB/DGLR Symposium Braunschweig, Germany, 2016 pp.51-60, 2016
[15] Savoni, L. and Rudnik, R., “Pylon Design for a Short Range Transport Aircraft with Over-the-Wing Mounted UHBR Engines”, 2018 AIAA Aerospace Sciences Meeting, AIAA SciTech Forum, (AIAA 2018-0011), 2018
[16] Wild, J., “AeroForce Aerodynamic Force Analyzer” Version 0.4, User manual, 1999